

# PHF20 is crucial for epigenetic control of starvation-induced autophagy through enhancer activation

Se Won Park<sup>1,†</sup>, Jaehoon Kim<sup>2,†</sup>, Sungryong Oh<sup>1,†</sup>, Jeongyoon Lee<sup>1</sup>, Joowon Cha<sup>1</sup>, Hyun Sik Lee<sup>1</sup>, Keun Il Kim<sup>3</sup>, Daechan Park<sup>2,4,\*</sup> and Sung Hee Baek<sup>1,\*</sup>

<sup>1</sup>Creative Research Initiatives Center for Epigenetic Code and Diseases, Department of Biological Sciences, Seoul National University, Seoul 08826, South Korea, <sup>2</sup>Department of Molecular Science and Technology, Ajou University, Suwon 16499, South Korea, <sup>3</sup>Department of Biological Sciences, Sookmyung Women's University, Seoul 04310, South Korea and <sup>4</sup>Department of Biological Sciences, Ajou University, Suwon 16499, South Korea

Received March 14, 2022; Revised June 15, 2022; Editorial Decision June 20, 2022; Accepted June 23, 2022

## ABSTRACT

Autophagy is a catabolic pathway that maintains cellular homeostasis under various stress conditions, including conditions of nutrient deprivation. To elevate autophagic flux to a sufficient level under stress conditions, transcriptional activation of autophagy genes occurs to replenish autophagy components. Thus, the transcriptional and epigenetic control of the genes regulating autophagy is essential for cellular homeostasis. Here, we applied integrated transcriptomic and epigenomic profiling to reveal the roles of plant homeodomain finger protein 20 (PHF20), which is an epigenetic reader possessing methyl binding activity, in controlling the expression of autophagy genes. *Phf20* deficiency led to impaired autophagic flux and autophagy gene expression under glucose starvation. Interestingly, the genome-wide characterization of chromatin states by Assay for Transposase-Accessible Chromatin (ATAC)-sequencing revealed that the PHF20-dependent chromatin remodelling occurs in enhancers that are co-occupied by dimethylated lysine 36 on histone H3 (H3K36me2). Importantly, the recognition of H3K36me2 by PHF20 was found to be highly correlated with increased levels of H3K4me1/2 at the enhancer regions. Collectively, these results indicate that PHF20 regulates autophagy genes through enhancer activation via H3K36me2 recognition as an epigenetic reader. Our findings emphasize the importance of nuclear events in the regulation of autophagy.

## INTRODUCTION

Autophagy is a highly conserved process that maintains cellular homeostasis by eliminating unnecessary proteins and damaged organelles (1,2). Under stress conditions such as nutrient starvation, autophagy is highly induced to perform a cytoprotective function (3,4). Since autophagy is essential for both cell survival and protection against various types of environmental damage, dysregulated autophagy can cause serious human diseases, including diabetes, neurodegenerative diseases, and cancer (5,6). As autophagy proceeds, the protein components of autophagosomes, along with their autophagy cargoes, are rapidly degraded by lysosomes (7,8). Thus, the transcription of autophagy components should be increased to avoid the depletion of the autophagosome and to maintain an optimal autophagic flux under cellular stress conditions (9,10). Previous studies have mainly reported the functions of transcription factors, including transcription factor EB (TFEB) and the forkhead box O (FOXO) protein family, to be involved in the regulation of autophagy (11–13). TFEB recognizes the CACGTG sequence in DNA (the 'CLEAR' motif), and activates the transcription of its specific target genes, including autophagy and lysosomal genes.

Gene expression is tightly regulated by not only transcription factors but also the chromatin structures that are modulated by chromatin remodelling factors (14). Post-translational modifications of histone tails influence the chromatin structures associated with transcriptional activation or repression. Active promoter regions are marked by H3K4me3, active enhancer regions are closely associated with H3K4me1 and H3K27ac, and heterochromatin regions are marked by H3K9me3 (15–21). The enzymes that induce or remove histone modifications (called writers and erasers, respectively) are orchestrated to establish

\*To whom correspondence should be addressed. Tel: +822 880 4413; Fax: +822 886 9078; Email: sbaek@snu.ac.kr  
Correspondence may also be addressed to Daechan Park. Tel: +8231 219 2514; Email: dpark@ajou.ac.kr

<sup>†</sup>The authors wish it to be known that, in their opinion, the first three authors should be regarded as Joint First Authors.

a specific repertoire of histone modifications under various cellular states (22–24). Most studies investigating the regulation of autophagy genes have focused on elucidating the mechanisms of writers and erasers (25–28). For example, H3R17me2 levels are increased by coactivator-associated arginine methyltransferase 1 (CARM1) under glucose starvation conditions, thereby leading to the activation of TFEB target genes (29). In contrast, H4K16ac levels are reduced by decreased Males absent on the first (MOF) histone acetyltransferase activity and sirtuin 1 activation upon autophagic stimulation. Given that epigenetic readers recognize specific histone modifications and exert their functions by bringing another effector complex to that site or by serving as an effector itself, elucidating the molecular functions of epigenetic readers is crucial for a comprehensive understanding of the regulation of autophagy genes (30–35).

PHF20, a member of the PHF family, contains two conserved Tudor domains and one plant homeodomain (PHD) (36). As a core component of MOF-nonspecific lethal (NSL) protein complex, PHF20 recognizes methylation of histone or non-histone targets and recruits NSL complex to target promoters, thereby enhancing histone H4 acetylation (37–40). PHF20 recognizes H3K4me2 through PHD and interacts with methyl residues on non-histone proteins, including estrogen receptor  $\alpha$ , p53, and p65 through Tudor domains (41–43). *Phf20*-deficient (*Phf20*<sup>-/-</sup>) mice show a high rate of perinatal lethality, with the surviving adults having a smaller body size than the wild-type (WT) mice, which is a well-known characteristic of autophagy-defective mice (44).

In this study, we found that *Phf20* deficiency leads to the failure to maintain autophagic flux under glucose starvation condition using genome-wide analyses, providing insights into the previously unrecognized epigenetic regulatory mechanism of PHF20 during autophagy.

## MATERIALS AND METHODS

### Reagents

The following antibodies were used: anti-Flag (F3165) and anti- $\beta$ -actin (A1978) (Sigma-Aldrich, St. Louis, MO, USA); anti-GFP (sc-9996) and anti-Lamin A/C (sc-6215) (Santa Cruz biotechnology, Dallas, TX, USA); anti-Tubulin (LF-PA0146A) (AbFrontier, Seoul, Korea); anti-PHF20 (#3934), anti-WDR5 (#13105), and anti-LC3 (#2775) (Cell Signaling Technology, Danvers, MA, USA); anti-HA (#MMS-101R) (Covance, Princeton, NJ, USA); Alexa Fluor 488 donkey anti-rabbit IgG (A21206) and Alexa Fluor 594 donkey anti-mouse IgG (A21203) (Invitrogen, Waltham, MA, USA). The following chemicals were used: hygromycin (H3274), puromycin (P8833), and CQ (C6628) (Sigma-Aldrich, St. Louis, MO, USA); Bafilomycin A1 (#11038) (Cayman, Ann Arbor, MI, USA); and rapamycin (R-5000) (LC laboratories, Woburn, MA, USA).

### Cell culture and transfection

We generated *Phf20*<sup>-/-</sup> immortalized mouse embryonic fibroblasts (MEFs) by using 3T3 protocol. WT and *Phf20*<sup>-/-</sup>

MEFs were cultured at 37 °C in Dulbecco's modified Eagle's medium (DMEM) (SH30243.01, HyClone, Marlborough, MA, USA) supplemented with 10% fetal bovine serum (FBS) (SH30084.03, HyClone) and ZellShield® (13-0050, Minerva biolabs, Hillsborough, NJ, USA) in a humidified incubator with 5% CO<sub>2</sub>. For glucose or amino acid starvation, cells were washed with pre-warmed Dulbecco's phosphate-buffered saline (DPBS) (SH30028.02, HyClone) and then exchanged media with glucose-free DMEM (LM001-56, Welgene, Gyeongsan-si, Korea) or amino acid-free DMEM (LM001-90, Welgene) supplemented with 10% dialyzed FBS (26400044, Gibco, Amarillo, TX, USA) and ZellShield®. Following reagents were used for cellular transfection: TurboFect (#R0531, ThermoFisher, Waltham, MA, USA) and Lipofectamine 3000 (L3000-001, Invitrogen). All cell lines were maintained without mycoplasma contamination.

### Lentivirus construction and production

3X Flag-PHF20 WT,  $\Delta$ Tudor and W97A mutants were cloned in pLVX vector, lentiviral shRNA constructs were cloned in pLKO.1 vector and guide RNA constructs for CRISPRi were cloned in lentiGuide-Puro (#52963, Addgene, Warrertown, MA, USA) vector. To generate lentivirus, constructs were co-transfected with virus packaging vectors (psPAX2 and VSV-G) in HEK293T cells. 48 h after transfection, virus containing media were collected and filtered through a 0.45  $\mu$ m-membrane filter. Lenti-X concentrator was added to filtered media according to the manufacturer's instructions (631231, Clontech, Mountain View, CA, USA). Collected virus was resuspended in DPBS and infected to cells with polybrene. Hygromycin selection was performed 10 days post-infection for pLVX vector and puromycin selection was performed 36 h post-infection for pLKO.1 vector. Following sequences were targeted by gRNA: *Atg13*: 5'-TGAGATGGTGTGTATAAATG-3' and 5'-CATTTATACACACCATCTCA-3'; *Ulk1*: 5'-ACTGACCCACTTAACTCATG-3' and 5'-CATGAGTTAAGTGGGTCAGT-3'.

### Preparation for obtaining whole-cell lysates

To harvest cells, cells were briefly rinsed with cold PBS and collected from the plate with scrapper. Then, cells were resuspended in EBC200 buffer (150 mM NaCl, 1% Triton X-100, 1% sodium deoxycholate, 0.1% sodium dodecyl sulfate (SDS), 50 mM Tris-HCl [pH 7.5], and 2 mM ethylenediaminetetraacetic acid (EDTA)) supplemented with protease inhibitors and sonicated using a Branson Sonifier 450 (Branson, Brookfield, CT, USA) at output 3 and a duty cycle of 30 for 10 pulses. Protein concentration in each lysate was quantified with the Bradford method and normalized with same concentration.

### Autophagic vacuole staining

Autophagic vacuoles were stained using the CYTO-ID® autophagy detection kit (ENZ-51031, Enzo Life Sciences, Farmingdale, NY, USA) and observed through fluorescence microscopy. Cells grown on coverslips at a density of  $2 \times 10^4$

cells were incubated with DMEM containing CYTO-ID® green detection reagent (1:500) and Hoechst 33342 (1:1000) at 37 °C for 30 min. After staining, the cells were washed with PBS and then fixed with 2% paraformaldehyde in PBS at 20–22°C for 10 min. Cells were then mounted and visualized under a confocal microscope (LSM700, Zeiss, Oberkochen, Germany).

### Immunofluorescence

Cells grown on coverslips at a density of  $5 \times 10^4$  cells were washed with PBS and then fixed with 2% paraformaldehyde in PBS at 20–22°C for 10 min. Fixed cells were permeabilized with 0.5% Triton X-100 in PBS (PBS-T) and incubated at 20–22°C for 10 min. Blocking was performed with 3% bovine serum in PBS-T for 1 h. For staining, the cells were incubated with antibodies at 20–22°C for 2 h, followed by incubation with fluorescent-labeled secondary antibodies for 1 h. Cells were then mounted and visualized under a confocal microscope (LSM700, Zeiss). For autophagy studies, MEFs were transfected with GFP-LC3 or mCherry-GFP-LC3 and sub-cultured onto coverslips. The following day, cells were incubated with complete media or glucose-starved media for 18 h.

### RNA purification and quantitative real-time PCR (qRT-PCR)

Total RNAs were purified with Trizol (15596026, Invitrogen). Purified RNAs were reverse-transcribed using SuPrimeScript cDNA Synthesis Kit (SRK-1000, GeNet-Bio, Daejeon, Korea). The reaction was performed with 2.5 µg of purified RNAs as template, Oligo dT and random hexamer for primer. Quantitative RT-PCR was reacted with SYBR TOPreal qPCR 2X PreMix (RT501, Enzynomics, Daejeon, Korea) following manufacturer's protocol. SYBR green signal was detected by an ABI prism 7500 system (Applied Biosystems, Waltham, MA, USA). Abundance of mRNA was quantified by the ddCt method using expression of HPRT, β-actin as control. All reactions were performed as triplicates. The primers used for qRT-PCR are listed in Supplementary Table S1.

### RNA-sequencing analysis

Total RNAs were extracted from WT and *Phf20*<sup>-/-</sup> MEFs with or without glucose starvation, respectively. Then, RNA-seq libraries were produced using Illumina's TruSeq Stranded mRNA LT Sample Prep Kit. After paired-end sequencing of the RNA-seq libraries, adapters and reads with low quality were filtered out by Trimmomatic (v0.36) (45). Then, the trimmed reads were aligned onto the mm10 genome reference using STAR (v2.5.3a) (46), and Transcripts Per Million (TPM) per gene was calculated by RSEM (v1.3.0) (47). The TPM values were log<sub>2</sub>-transformed for downstream analyses such as hierarchical clustering, *k*-means clustering and functional analysis. *k*-means clustering was performed to identify the genes regulated by PHF20, and DAVID (v6.8) (48) was utilized for gene ontology. For Gene Set Enrichment Analysis (GSEA)

(v4.0.3) (49), mm10 annotated protein coding genes were mapped to human protein coding genes using biomaRt (v2.40.5) (50) in R. Phenotype label was assigned as 1:3:1:1 for WT MEFs normal condition: WT MEFs glucose starvation: *Phf20*<sup>-/-</sup> MEFs normal condition: *Phf20*<sup>-/-</sup> MEFs glucose starvation, and genes were ranked by the Pearson correlation coefficient. Finally, C2 and C5 gene sets in MSigDB (molecular signatures database) (v7.0) (51,52) of the Broad Institute were used for the enrichment score.

### Assay for transposase-accessible chromatin using sequencing (ATAC)-sequencing analysis

ATAC-seq libraries were prepared for sequencing using Illumina Tagment DNA TDE1 Enzyme and Buffer Kits (#20034197, Illumina, San Diego, CA, USA) and paired-end sequencing was performed by Illumina platform. Then, paired-end reads were aligned onto mm10 using Burrows-Wheeler Alignment tool (BWA) (v0.7.12) (53) and peak calling was conducted by Model-based Analysis for ChIP-Seq (MACS) (v2.1.2) (54). For hierarchical clustering based on the peak intensities, the significant peaks were selected with a cut-off false discovery rate (FDR) 0.01 for each sample then merged across the samples. Reads per peak, as an intensity, was counted using BEDTools (v2.25.0) (55). To identify differentially opening peaks (DOPs) between samples, DESeq2 (v1.26.0) (56) was applied for the intensities. For average profile of DOPs, normalized read counts centered on peak summits were calculated and plotted by deepTools2 (v3.1.1) (57).

### Purification of GST-fusion proteins and *in vitro* peptide binding assay

GST-tagged PHF20 Tudor 1 and 2 domains (Tudor 1&2, 1–147 a.a) of WT or W97A mutant constructs were cloned in pGEX-4T-1 vector and were transformed in Rosetta *Escherichia coli* strain. The protein was purified with glutathione beads (GE17-0756-01, GE Healthcare, Chicago, IL, USA) and eluted with elution buffer (50 mM Tris-HCl [pH 7.5], 100 mM NaCl, 10 mM reduced glutathione, and 1 mM DTT supplemented with 1X complete protease inhibitor). For *in vitro* peptide binding assay, 2 µg of WT and W97A purified proteins were incubated overnight with 1 µg of biotin-labeled protein peptides in the 300 µl of binding buffer (50 mM Tris-HCl [pH 7.5], 200 mM NaCl, and 0.05% NP-40). Then, 30 µl of streptavidin sepharose beads were added to each tube and incubated for 1 hr. After binding, beads were washed 4 times with binding buffer and samples were boiled with 30 µl of SDS sampling buffer.

### *In vitro* histone peptide binding array

*In vitro* histone peptide binding array was performed with MODified™ Histone Peptide Array Kit (13001, Active Motif, Carlsbad, CA, USA) following manufacturer's protocol. In brief, array kit was blocked with 5% milk in TTBS (10 mM Tris-HCl [pH 7.5], 150 mM NaCl and 0.05% Tween-20) at 4°C overnight. After that, the kit was incubated with

purified GST-PHF20 Tudor 1&2 WT protein in binding buffer (20 mM HEPES [pH 7.9], 100 mM KCl, 1 mM EDTA, 10% glycerol, and 0.1 mM DTT) for 1 h. Then, primary GST antibody and secondary antibody were treated and bound GST proteins were detected with ECL solution.

### Chromatin immunoprecipitation (ChIP) assay

Before crosslinking, cells were washed three times with cold PBS to remove amine-containing proteins from cells and media. Then, ethylene glycolbis(succinimidylsuccinate) (EGS) was treated to the cell for final concentration of 2 mM at 20–22°C. After 20 min, 1% formaldehyde was added and cells were incubated for 10 min. After glycine quenching, cells were harvested and resuspended with ChIP lysis buffer containing 50 mM Tris-HCl [pH 8.1], 10 mM EDTA, 1% SDS and protease inhibitor cocktail. DNA was fragmented with sonication until average size reaches 250 bp. Dilution buffer containing 20 mM Tris-HCl [pH 8.1], 150 mM NaCl, 2 mM EDTA and 1% Triton X-100 were added to chromatin extract with a volume of ten times. Diluted samples were subjected to immunoprecipitation with assigned antibodies overnight at 4°C. Then, 40 µl of Protein A/G sepharose beads were added to capture immunocomplexes. After 2 h of incubation at 4°C, beads were washed with TSE I buffer (20 mM Tris-HCl [pH 8.1], 0.1% SDS, 1% Triton X-100, 2 mM EDTA and 150 mM NaCl), TSE II buffer (20 mM Tris-HCl [pH 8.1], 0.1% SDS, 1% Triton X-100, 2 mM EDTA and 500 mM NaCl), buffer III (10 mM Tris-HCl [pH 8.1], 0.25 M LiCl, 1% NP-40, 1% deoxycholate and 1 mM EDTA), three times TE buffer (10 mM Tris-HCl [pH 8.0] and 1 mM EDTA). Immunocomplex was eluted from beads by incubation with elution buffer (1% SDS and 0.1 M NaHCO<sub>3</sub>) for 2 hr and the elute was reverse crosslinked by overnight incubation at 65°C. RNAs and proteins in sample were digested with RNase and protease K. Final samples and matched input samples were analyzed with quantitative-RT PCR or subjected to construct sequencing libraries. The primers used for qRT-PCR are listed in Supplementary Table S1.

### Chromatin immunoprecipitation (ChIP)-sequencing analysis

Paired-end reads were aligned onto the mm10 reference genome using BWA (v0.7.12), and MACS (v2.1.2) was utilized to identify significant peaks with cut-offs of false discovery rate (FDR) 0.01 and signal value 5.

### CUT&RUN assay

CUT&RUN assay kit (#86652, Cell Signaling) was used following manufacturer's instruction. In brief, collected cells were washed with wash buffer and permeabilized with Digitonin solution. Then, cells were bound to Concanavalin A magnetic beads and incubated with antibody overnight at 4°C. Next, pAG-MNase was treated to fragment DNA where target protein is attached. DNA extract was purified with DNA Purification Buffers and Spin Columns (#14209, Cell signaling) and subjected to qRT-PCR. The primers used for qRT-PCR are listed in Supplementary Table S1.

### Chromosome conformation capture (3C) assay

The 3C assays were performed as modified version of previous methods (58,59). In brief,  $1 \times 10^7$  cells were crosslinked in 1% formaldehyde/media for 10 min at 20–22°C. After crosslinking step, glycine was added to a final concentration of 0.125 M and incubated for 10 min. After washing with DPBS for 2 times, cells were harvested and lysed with Buffer I (10 mM HEPES [pH 6.5], 0.25% Triton X-100, 10 mM EDTA and 0.5 mM EGTA) and Buffer II (10 mM HEPES [pH 6.5], 200 mM NaCl, 1 mM EDTA, and 0.5 EGTA) at 4°C for 5 min, respectively. Cells were additionally lysed with lysis buffer (10 mM Tris-HCl [pH 7.5], 10 mM NaCl, 0.2% NP-40 and 1× complete protease inhibitor). After centrifugation, the pelleted nuclei were resuspended with 1.2× restriction enzyme buffer M (Takara, Kusatsu, Japan) with 0.3% (w/v) SDS and incubated at 37°C while shaking at 900 r.p.m. Triton X-100 was added to a final concentration of 2% (v/v) and incubated at 37°C while shaking at 900 r.p.m. 400 U of restriction enzyme HindIII (1060BH, Takara) was added and incubated overnight at 37°C while shaking at 900 r.p.m. for chromatin digestion. For restriction enzyme inactivation, SDS was added to a final concentration of 1.6% and samples were incubated for 20 min at 65°C while shaking at 900 r.p.m. Before ligation, 1.15× filtered ligation buffer (66 mM Tris-HCl [pH 7.5], 5 mM DTT, 5 mM MgCl<sub>2</sub> and 1 mM ATP) and 1% Triton X-100 was added and were incubated for 1 h at 37°C while shaking gently. The DNA was ligated by 100U T4 DNA ligase (M053L, Enzymatics) at 16°C for 4 h followed by 30 min incubation at 20–22°C. 300 µg of Protease K (P2308, Sigma-aldrich) was added and the DNA was de-crosslinked at 65°C overnight. DNA purification was performed by phenol-chloroform extraction and ethanol precipitation. The following PCR program was used: 95°C for 10 min, followed by 38 cycles of 95°C for 10 s, 60°C for 10 s, and 72°C for 10 s. The following primers were used.

Atg13 promoter fwd (P)  
5'-ACTGTTTTGAAAGCGGGTTG-3';  
Atg13 enhancer fwd (E)  
5'-CGGTTGGTTCCTTGTGAATC-3';  
Ulk1 promoter rev (P)  
5'-TCCCCACAGTTTTTGGTTTC-3';  
Ulk1 enhancer rev (E)  
5'-TACCCACAGGGCCATCTTTA-3';  
Supt5 promoter rev (P)  
5'-GAGCAGGCCCTAAAGTCTC-3';  
Supt5 enhancer rev (E)  
5'-TGGCTTTTTTAAACCGTGAGG-3';

### Statistical analysis

All experiments were performed independently at least three times. Prism v5 software (GraphPad) was used for statistical analysis. Student's *t*-test was used for comparison between two groups. Analysis of variance (ANOVA) with post hoc tests was used for comparison of multiple samples and discrimination of significant relationships. *P*-values <0.05 were considered statistically significant.

## RESULTS

### PHF20 is crucial for starvation-induced autophagy

As the phenotypes of *Phf20*<sup>-/-</sup> mice showing perinatal lethality are often observed for autophagy-defective mice, we tested the possibility that PHF20 is involved in autophagy. To detect autophagic activity, we analyzed the conversion of non-lipidated light chain 3 (LC3)-I form to lipidated LC3-II form, which is a common marker of autophagic occurrence. We induced autophagy in WT and *Phf20*<sup>-/-</sup> mouse embryonic fibroblasts (MEFs) by glucose and amino acid starvation, and found that LC3-II conversion in *Phf20*<sup>-/-</sup> MEFs was attenuated as compared to that in WT MEFs under both glucose and amino acid starvation conditions (Figure 1A and 1B). The same results were observed upon rapamycin treatment, which induces autophagy by inhibiting mammalian target of rapamycin (mTOR) (Figure 1C). The formation of green fluorescent protein (GFP)-tagged LC3-positive autophagosomes was examined to evaluate the role of PHF20 in autophagy. Upon glucose starvation, the number of GFP-LC3 punctate cells increased in WT MEFs, however, this increase in number of puncta was attenuated in *Phf20*<sup>-/-</sup> MEFs (Figure 1D).

Next, we compared the autophagic flux between WT and *Phf20*<sup>-/-</sup> MEFs by treating the cells with lysosomal inhibitors that prevent the degradation of the mature autophagosome. We treated WT and *Phf20*<sup>-/-</sup> MEFs with chloroquine (CQ) and compared the induction of autophagic flux in the cells under glucose starvation (Figure 1E). While the autophagic flux in WT MEFs was greatly increased by glucose starvation, *Phf20*<sup>-/-</sup> MEFs failed to show significant increase in autophagic flux (Figure 1E). Similar results were observed in the absence or presence of Bafilomycin A treatment with Cyto-ID staining, which is an autophagosome-specific fluorescent reporter (Figure 1F). The number of autophagosomes was increased to a much higher extent by glucose starvation in WT MEFs than in *Phf20*<sup>-/-</sup> MEFs. Thereafter, we used the mCherry-GFP-LC3 reporter to examine the total number of autophagosomes induced and the extent of autophagic flux at the same time. During the formation of an autophagosome, mCherry-GFP-LC3 conjugates with the autophagosome membrane and stains the vesicle yellow, which results from the fluorescence of both mCherry and GFP. After a lysosome fuses with an autophagosome to form an autolysosome, only red fluorescence is observed, because the fluorescent activity of GFP is vulnerable to the acidic environment. Consecutively, WT MEFs showed increased number of both yellow and red puncta under glucose starvation, whereas *Phf20*<sup>-/-</sup> MEFs had significantly attenuated number of both puncta (Figure 1G). Therefore, these results indicate that *Phf20* deficiency impairs the induction of autophagic flux under glucose starvation.

### PHF20 functions as a transcriptional coactivator of autophagy genes

To examine the role of PHF20 in autophagy at the transcriptional level, we carried out RNA-sequencing (RNA-seq) of WT and *Phf20*<sup>-/-</sup> MEFs with or without glucose

starvation (Figure 2A). In unsupervised hierarchical clustering, the *Phf20*<sup>-/-</sup> MEFs were closely clustered independent of the starvation conditions, thereby suggesting that *Phf20* deletion eliminates the transcriptional responses to glucose starvation (Figure 2B). We then performed *k*-means clustering (*k* = 8) to figure out the functional role of PHF20 in regulating gene expression (Figure 2C and Supplementary Table S2). The genes in cluster 1 were expressed in a PHF20-dependent manner, as the deletion of *Phf20* led to the failure of activation of the genes in WT MEFs upon glucose starvation (Figure 2D and Supplementary Figure S1). Interestingly, gene ontology (GO) analysis revealed that autophagy genes were significantly represented in cluster 1, indicating that PHF20 is involved in transcriptional activation of autophagy genes (Figure 2E and Supplementary Table S3).

Next, we conducted gene set enrichment analysis (GSEA) by ranking the genes based on Pearson correlation coefficient in a PHF20-dependent manner. The results confirmed that the gene sets of the autophagic process were significantly enriched in the PHF20-dependent cluster (Figure 2F). Furthermore, we observed that the activation of genes related to autophagy initiation, phagophore expansion, and cargo recruitment and trafficking (85) in WT MEFs upon glucose starvation was repressed by *Phf20* deletion, thereby showing the transcriptional dependency of autophagy on PHF20 (Figure 2G). We further validated the function of PHF20 in transcriptional regulation using quantitative real-time polymerase chain reaction (qRT-PCR) for the genes associated with autophagy such as those encoding the autophagy (Atg) family proteins and the autophagy receptor sequestosome 1 (*Sqstm1*), also known as p62 (Figure 2H). Taken together, the results of gene expression profiling revealed that PHF20 acts as a transcriptional coactivator during autophagy on a transcriptome-wide scale.

### PHF20 modulates autophagy genes through enhancer activation

As PHF20 is a chromatin-binding protein, we carried out ATAC-seq to elucidate the role of PHF20 in the alteration of chromatin structures during autophagy (Figure 3A). After peak calling for open chromatin regions in ATAC-seq, hierarchical clustering using the peak intensities showed that clusters were segregated between WT and *Phf20*<sup>-/-</sup> (Figure 3B). The dendrogram in Figure 3B indicates that open chromatin structures were globally altered by *Phf20* deletion, whereas the effect of glucose starvation on chromatin structures was relatively minimal. We then identified differentially opening peaks (DOPs) between WT and *Phf20*<sup>-/-</sup> under each condition. We observed that 16,976 and 20,906 peaks were significantly changed by *Phf20* deletion under normal and glucose starvation condition, respectively (Figure 3C). Next, we conducted GO term analysis on the genes which show starvation-induced chromatin opening peaks (Figure 3D and Supplementary Table S4). The results showed that autophagy-related GO terms were significantly represented in WT MEFs, indicating a PHF20-dependent chromatin opening of autophagy-related genes under glucose starvation.

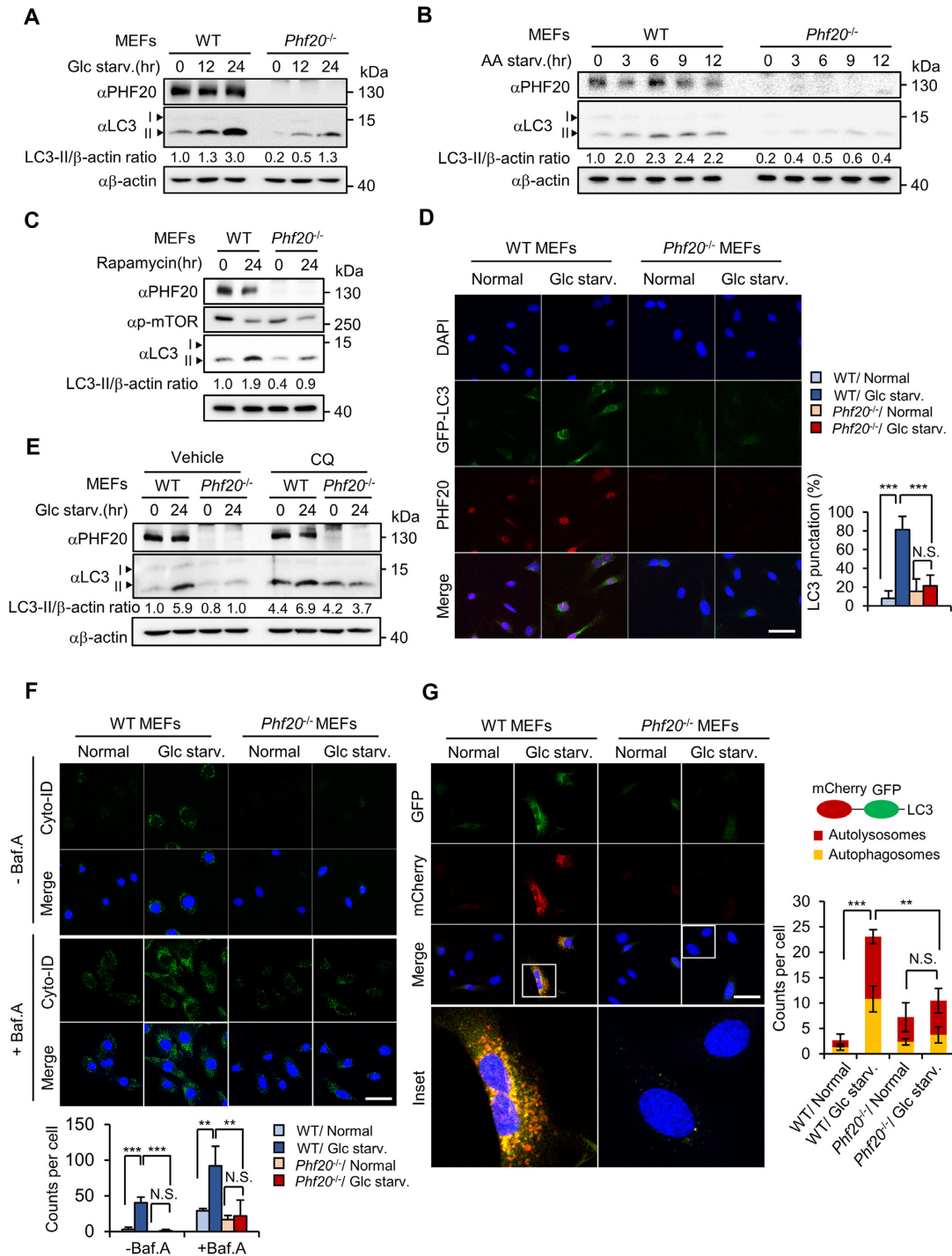


**Figure 1.** PHF20 is crucial for inducing autophagic flux under glucose starvation. (A–C) Immunoblot analysis of light chain 3 (LC3) levels in cell lysates of WT or *Phf20*<sup>-/-</sup> MEFs after glucose starvation (A), amino acid starvation (B), and rapamycin (150 nM) treatment (C). The number below indicates LC3-II/β-actin ratio. (D) Representative confocal images of GFP-LC3 puncta formed under control or glucose starvation conditions. Scale bar, 50 μm. The graph indicates the number of LC3-positive cells. Bars, mean ± standard error of the mean (SEM); \*\*\* *P* < 0.001. Statistical analysis using two-tailed *t*-test. (E) Autophagic flux was analyzed in WT or *Phf20*<sup>-/-</sup> MEFs in the presence or absence chloroquine (10 μM; 4 h) under glucose starvation conditions. The LC3-II/β-actin ratio is indicated. (F) Representative confocal images of autophagic vacuoles in WT or *Phf20*<sup>-/-</sup> MEFs in the presence or absence of bafilomycin A1 (200 nM; 2 h). Autophagic vacuoles were detected using the CYTO-ID staining. Nucleus are stained with Hoechst (Blue). Scale bar, 50 μm. The graph indicates the number of autophagic vacuoles per cells. Bars, mean ± SEM; \*\* *P* < 0.01, \*\*\* *P* < 0.001. Statistical analysis using two-tailed *t*-test. (G) Representative confocal images of mCherry-GFP-LC3 assays in WT or *Phf20*<sup>-/-</sup> MEFs. Colocalization of mCherry and GFP signal (yellow puncta) represents autophagosomal vesicles that have not fused with a lysosomal compartment (phagophores or autophagosomes). mCherry signal without GFP signal (red puncta) represents acidic autophagosomal vesicles (acidic amphisomes or autolysosomes). Nucleus are stained with DAPI (Blue). Scale bar, 50 μm. The graph indicates the number of puncta per cell. Bars, mean ± SEM; \*\* *P* < 0.01, \*\*\* *P* < 0.001. Statistical analysis using two-tailed *t*-test.

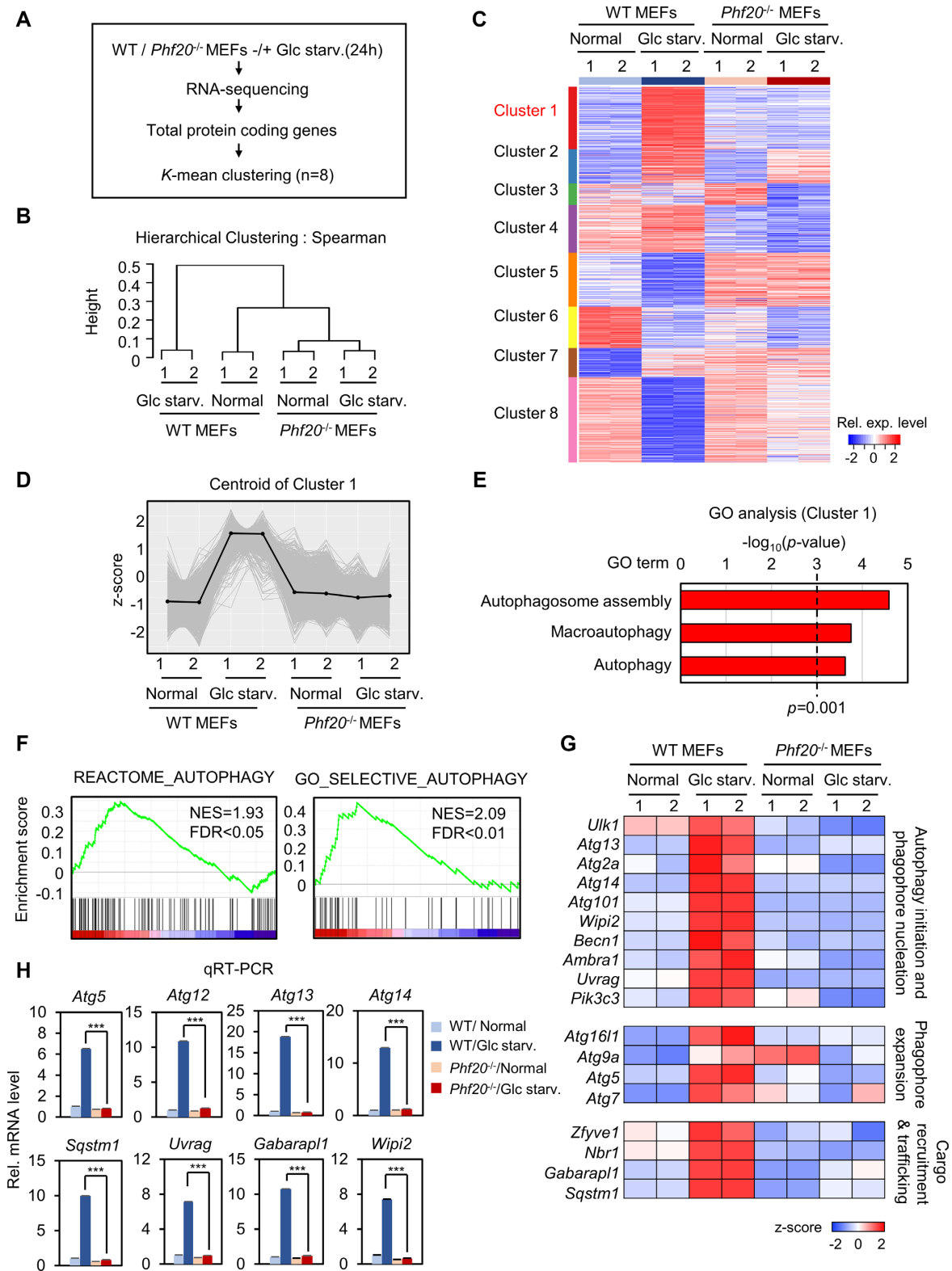


**Figure 2.** PHF20 induces autophagy genes under glucose starvation. **(A)** Workflow of RNA-sequencing and downstream analysis. **(B)** Unsupervised hierarchical clustering using top 10% variably expressed genes. The y-axis shows distance in Spearman correlation coefficient. **(C)** Heat map of  $k$ -means clustering of total protein coding genes in WT and  $Phf20^{-/-}$  with or without glucose starvation ( $n = 12208$ ,  $k = 8$ ). The genes are clustered in 8 different groups based on relative gene expression across the samples. Cluster 1 which shows PHF20 dependent gene activation pattern is highlighted in red. **(D)** z-score centroids of Cluster 1. The black line and grey lines indicate the centroid and genes, respectively. **(E)** Functional Gene Ontology (GO) analysis on the genes in Cluster 1. Autophagy related terms are shown significantly in Cluster 1 but not in other clusters. **(F)** Gene Set Enrichment Analysis (GSEA) for the genes correlated with the gene expression in Cluster 1. FDR, false discovery rate; NES, normalized enrichment score. **(G)** Expression levels of genes involved in autophagy initiation, phagophore expansion, and cargo recruitment and trafficking. **(H)** mRNA expression of autophagy-related genes with quantitative real time-PCR (qRT-PCR). Bars, mean  $\pm$  SEM; \*\*\*  $P < 0.001$ . Statistical analysis using two-tailed  $t$ -test.

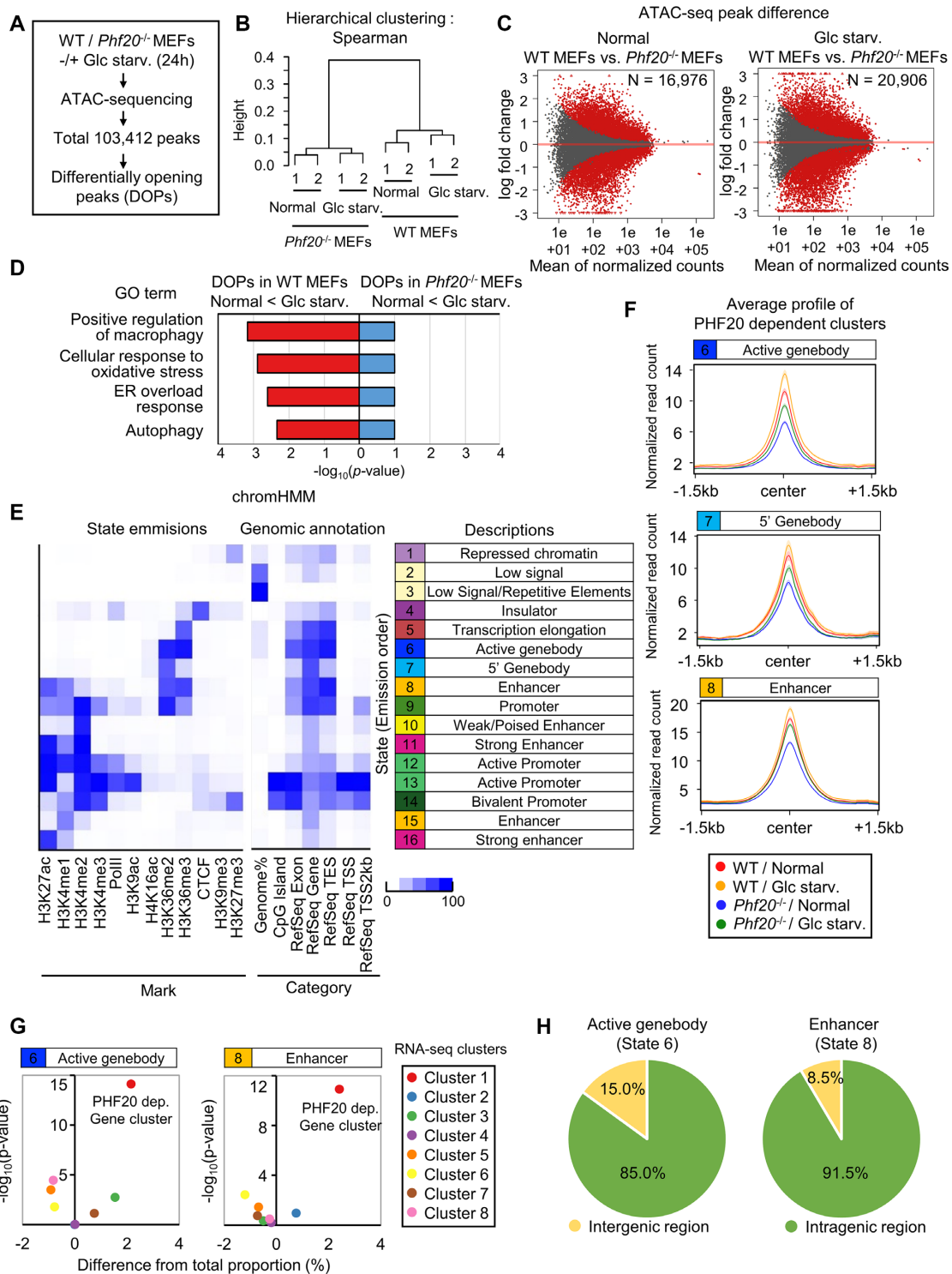


**Figure 3.** PHF20 affects chromatin opening of intragenic enhancer regions. (A) Workflow of ATAC-sequencing analysis. (B) Unsupervised hierarchical clustering using top 10% variably opened peaks (Spearman distance). The height implies similarity of opening peaks by each sample. (C) Differentially opening peaks (DOPs) between WT and *Phf20*<sup>-/-</sup> under each condition. Red dots represent statistically significant DOPs that are less than adjusted *P*-value 0.05. N, the number of DOPs that are greater than fold change 2 and less than adjusted *P*-value 0.05. (D) Functional analysis for the DOPs between conditions. GO results are shown for the genes whose TSS are within 10 kb from the DOPs. Autophagy-related terms are significantly found in WT but not *Phf20*<sup>-/-</sup>. (E) Chromatin state using chromHMM software. Each row represents one chromatin state. From left to right: Histone mark and probability used to define the states (State emission). Chromatin state enrichment in genomic features (genomic annotation). Description of 16 states (Descriptions). (F) Average plots of DOPs in state 6, 7 and 8 by each sample. (G) Comparing the chromHMM state ratio of DOPs in each RNA-sequencing cluster to the ratio of DOPs (*n* = 33 443) in total protein-coding genes. DOPs distributed under 50 kb from TSS are counted. Statistical analysis using chi-square test. Total protein-coding genes have 4.43% (*n* = 1481 from 33 443 total DOPs, <50 kb) of state 6 DOPs, and 7.54% (*n* = 2521 from 33 443 total DOPs, <50 kb) of state 8 DOPs. (H) Proportion of DOPs at genomic location. DOPs in states 6 and 8 are enriched in the intragenic region.

To investigate precisely which chromatin states were regulated by PHF20 on a genome-wide scale, we utilized chromHMM, which is a software for discovering chromatin states by learning chromatin signatures based on the multivariate Hidden Markov Model (60,61). We collected 12 different publicly available ChIP-seq datasets, such as RNA polymerase II and CTCF ChIP-seq datasets, and various histone ChIP-seq datasets derived from studies using MEFs (Figure 3E). After learning the diverse chromatin signatures, we were able to generate genome-wide chromatin annotations consisting of 16 states (Supplementary Table S5). To specify the chromatin states regulated by PHF20, we calculated the average profile of the DOPs for each state (Figure 3F and Supplementary Figure S2). We found that states 6, 7 and 8 show relatively strong dependency on PHF20 for starvation-induced chromatin opening, defining PHF20 dependency as states where chromatin became less accessible by *Phf20* depletion under glucose starvation. The state 3 was excluded because it was a repetitive region and had no significant signal of all histone marks. Regarding the states 4, 5 and 9, they exhibited relatively weak PHF20 dependency, meaning that the chromatin accessibility difference (WT Glc starv - KO Glc starv) was smaller. As a result, we finally defined the states 6, 7 and 8 as PHF20-dependent states (Figure 3F, Supplementary Figure S2 and S3). Based on the opened patterns of the DOPs along with the chromHMM states, we hypothesized that DOPs in states 6, 7 and 8 lead to the PHF20-dependent gene expression under glucose starvation. To confirm this, we performed an integrative analysis of ATAC-seq with the gene clusters from RNA-seq, which were distinguished by PHF20-dependent gene expression patterns. First, we counted the number of DOPs within 50 kb from the transcriptional start site (TSS) of each gene. Next, we compared the proportions of DOPs between RNA-seq clusters. Interestingly, states 6 and 8 had greater proportion of DOPs in the RNA-seq cluster with PHF20-dependent expression (cluster 1) (Figure 3G), indicating that PHF20-dependent expression is regulated by DOPs in states 6 and 8 near their TSSs (<50 kb). Further, we investigated the genomic regional distribution of the DOPs in states 6 and 8. Interestingly, DOPs belonging to PHF20-dependent states 6 and 8 are more condensed in intragenic regions, suggesting that PHF20 is mainly associated with chromatin opening of intragenic regions (Figure 3H). Collectively, these results indicate that PHF20 activates its target DOPs under glucose starvation, and activation of these DOPs is closely related to the PHF20-dependent expression of autophagy genes.

### ***Phf20* deletion reduces active enhancer markers on its target DOPs**

Since the chromHMM showed that PHF20-dependent DOPs are localized in non-promoter regions, including an H3K4me-enriched enhancer state (state 8: Enhancer region as shown in Figure 3E), we hypothesized that PHF20 is required for the activation of *cis*-regulatory elements to upregulate autophagy-related genes upon glucose starvation. To test this hypothesis, we performed ChIP-seq for H3K4me1 and H3K4me2, which are known to be closely linked to active *cis*-regulatory elements. Average profiling

and read density heatmaps around the peak center revealed that the levels of both H3K4me1 and H3K4me2 increased on PHF20 dependently opened chromatin regions in WT MEFs, but not in *Phf20*<sup>-/-</sup> MEFs upon glucose starvation (Figure 4A and B). In particular, the DOPs near the *Supt5*, *Ulk1*, and *Atg13* loci showed marked chromatin opening during autophagy, along with H3K4me1 and H3K4me2 enrichment in WT, but not in *Phf20*<sup>-/-</sup> MEFs (Figure 4C). Moreover, these three DOPs are closely located to the state 8 enhancer region of chromHMM which shows a PHF20-dependent opening pattern.

### **PHF20 activates enhancers via the recognition of H3K36me2 and the recruitment of mixed lineage leukemia 3/4 (MLL3/4) complex**

Since the PHF20-dependent chromatin states show a high level of H3K36 methylation as determined by the chromHMM analysis (Figure 5A), we tested the possibility that PHF20 is responsible for chromatin opening at the H3K36me-enriched regions during autophagy. For this, we first examined whether PHF20 recognizes H3K36 methylation directly. Crystal structure of PHF20 predicted that the Tudor domain of PHF20 has a potential for binding di-methylated histone substrates including H3K36me2 (62). Moreover, the comparison of the 3D structure of the PHF20 Tudor domain with that of H3K36me2-bound PHF1 Tudor domain from structural modeling allowed us to predict that the PHF20 Tudor domain possesses an aromatic cage structure to be able to accommodate H3K36me2 binding as in the case of PHF1 Tudor domain (63). Therefore, we tested the binding affinity of GST-PHF20 Tudor 1 and 2 domains (Tudor 1&2) to various histone modifications using an *in vitro* histone peptide binding array (Figure 5B). The peptide binding array revealed specific binding of PHF20 Tudor 1&2 to H3K36me2 as well as other di-methylated lysine peptides (Figure 5C). Next, we performed an *in vitro* peptide binding assay to examine the binding affinity of GST-PHF20 Tudor 1&2 using WT and mutant W97A; the mutant W97A carries a mutation corresponding to a core aromatic residue to block substrate binding to H3K36me2. GST-PHF20 Tudor 1&2 of WT protein, but not W97A mutant protein, selectively bound the H3K36me2 peptide (Figure 5D). To test the effect of H3K36me2 binding affinity on the recruitment of PHF20, we conducted the CUT & RUN assay, a chromatin immunocleavage assay with a primary antibody and micrococcal nuclease conjugated with protein A (pA-MN) (64,65), with Flag-PHF20 WT and  $\Delta$ Tudor mutant (Figure 5E). While the binding of PHF20 WT on the target site increased upon glucose starvation, the  $\Delta$ Tudor mutant which cannot bind H3K36me2 failed to show increased recruitment upon glucose starvation (Figure 5F).

Next, we tried to find out the effector molecules that directly activate the H3K36me2-enriched enhancer regions, given that PHF20 has no enzymatic activity. Since the MLL complexes are well-known methyltransferase complexes for both H3K4me1 and H3K4me2 (66–70), we examined the interaction between PHF20 and MLL components including WDR5 and RbBP5. Co-immunoprecipitation assay revealed that WDR5 and RbBP5 showed comparable binding

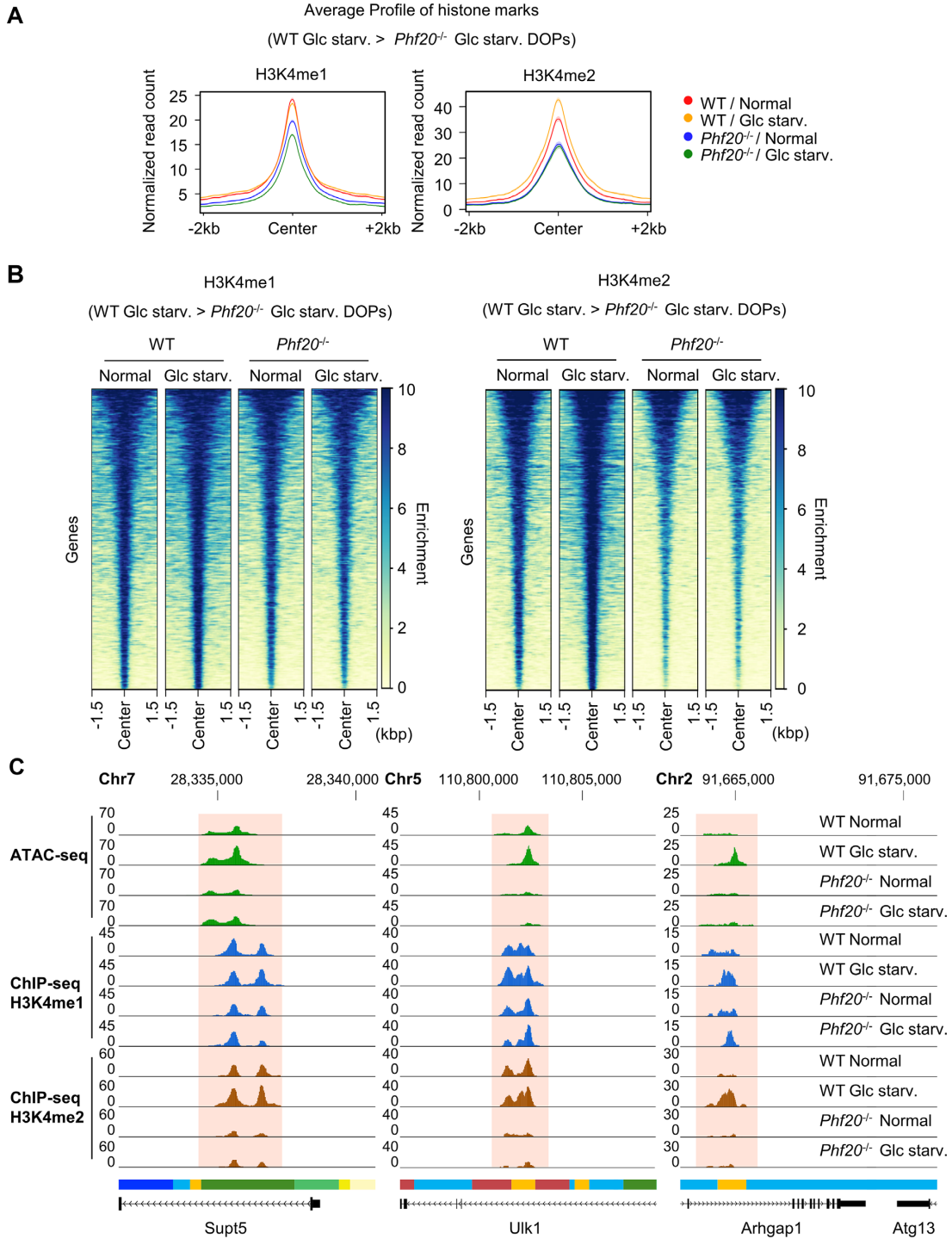


**Figure 4.** *Phf20* deletion reduces active enhancer markers on its target DOPs. (A) Average profiles of H3K4me1 and H3K4me2 signals in WT Glc starv. > *Phf20*<sup>-/-</sup> Glc starv. DOPs for each condition. (B) Read density heatmaps around peak center of H3K4me1 and H3K4me2 signals in WT Glc starv. > *Phf20*<sup>-/-</sup> Glc starv. DOPs for each condition. (C) UCSC Genome Browser (GB) tracks of ATAC-seq signal (green), ChIP-seq signals for H3K4me1 (blue) and H3K4me2 (darkbrown), and chromHMM chromatin states around the DOPs of *Supt5*, *Ulk1* and *Atg13*. Y-axis represents normalized read counts.

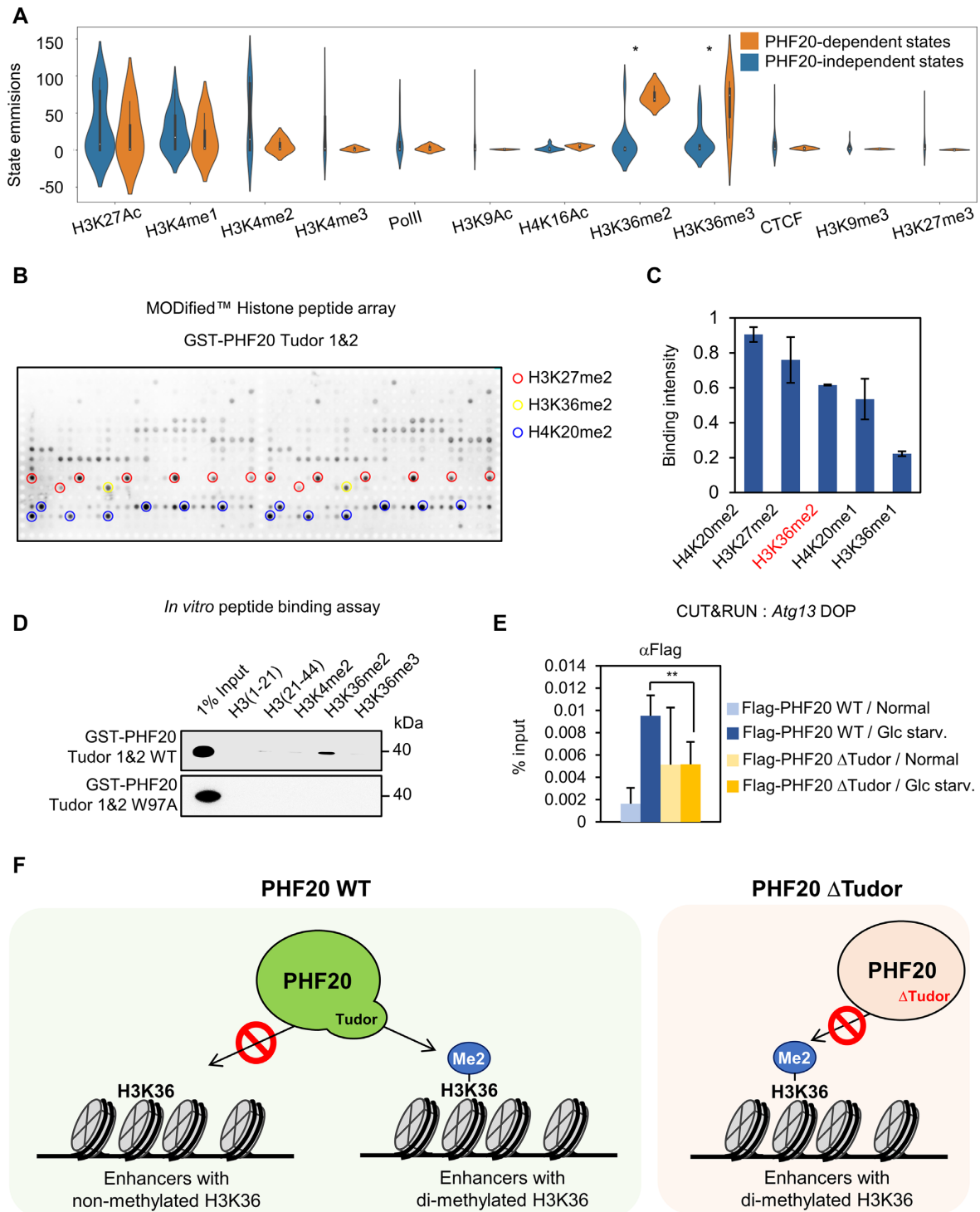


**Figure 5.** PHF20 recognizes H3K36me2 via its Tudor 1 and 2 domains. (A) Relative H3K36me2 ChIP-seq peak intensity of PHF20-dependent (states 6 and 8) and PHF20-independent states in chromHMM. (B) Screening for histone peptide binding of PHF20 Tudor 1 and 2 domains (Tudor 1&2) with MODified™ Histone Peptide Array. GST-PHF20 Tudor 1&2 construct was detected with GST antibody. Histone peptides with significant binding intensity are indicated with red, yellow, and blue circles. Each dot indicated with the color contains the following histone peptides. red:H3K27me2, yellow:H3K36me2, and blue:H4K20me2. (C) Top five histone peptides with the highest binding intensity. Binding intensity was calculated with MODified™ Histone Peptide Array analysis program. (D) *In vitro* peptide binding assay using GST-PHF20 Tudor 1&2 of WT and W97A constructs was performed, followed by immunoblot analysis with anti-GST antibody. (E) CUT&RUN assay of Flag-tagged PHF20 constructs on *Atg13* DOP region. (F) Schematic model for H3K36me2 recognition of PHF20 WT and Tudor domain deletion mutant.

to PHF20 under glucose starvation (Figure 6A). Moreover, PHF20 interacted with KDM6A/UTX, a specific component of MLL3/4 complex, but not with Menin, a specific component of MLL1/2 complex, indicating that PHF20 has a binding preference for MLL3/4 complex (Figure 6B). Because MLL3/4 complex are known to play an important role in establishing H3K4me1 on enhancer, this result supports that PHF20 is mainly responsible for enhancer activation upon glucose starvation. To test whether PHF20 recruits the MLL3/4 complex to H3K36me2-enriched target sites under glucose starvation, we performed ChIP assay and checked the recruitment of WDR5 to PHF20-dependent DOPs (Figure 6C). WDR5 was recruited to the target DOPs under glucose starvation in WT MEFs, but not in *Phf20*<sup>-/-</sup> MEFs. Moreover, the transcription of eRNA, which is closely correlated with enhancer activity (71,72), increased under glucose starvation in WT MEFs, but not in *Phf20*<sup>-/-</sup> MEFs (Figure 6D). Next, we tested the effect of PHF20-dependent enhancer activity on its target gene expression using CRISPRi. We used a fusion protein of the enzymatically inactive dCas9 and Krüppel-associated box (KRAB) repressor (dCas9-KRAB) to repress the target enhancer regions (73). Inhibition of the enhancer region by CRISPRi led to a decrease in target gene expression exemplified by *Atg13* and *Ulk1* without affecting promoter activity (Figure 6E and F). At last, we confirmed the PHF20 dependent promoter-enhancer looping with chromosome conformation capture (3C) assay (Figure 6G-I). The looping between the PHF20 dependent target gene promoters and DOP regions increased under glucose starvation in WT MEFs, but not in *Phf20*<sup>-/-</sup> MEFs. Taken together, our data indicate that PHF20 increases the expression of autophagy genes via enhancer activation by recruiting the MLL3/4 complex to the target DOPs under glucose starvation (Figure 7).

## DISCUSSION

Replenishment of autophagy proteins by transcriptional activation is an essential process for prolonged autophagy. This process is achieved by maintaining adequate levels of autophagic flux. To precisely control the expression of specific target genes, epigenetic regulation is crucial. Here, we defined the integrated signaling pathway that connects the upstream inducing signal of autophagy to the downstream target gene expression through epigenetic regulation. Genome-wide analyses and molecular mechanistic studies revealed that PHF20 functions as a versatile platform for recruiting MLL3/4 methyltransferase complexes with increased histone H3K4 methylation and the subsequent activation of autophagy genes. Integrative analysis of RNA-seq and ATAC-seq results showed that PHF20 altered the chromatin structure to activate the transcription of autophagy-related genes on a genome-wide scale and the global chromatin opening by PHF20 was more prominent under glucose starvation. With respect to its region of activity on the genome, enhancers and gene bodies were the chromatin states where PHF20 evidently worked, suggesting that PHF20 is likely associated with long range interactions in the 3D genome structure (Figure 7). These specificities of PHF20 for chromatin states were found to be achieved

by interaction with the modified histone marks. Therefore, our genome-wide approaches indicate that epigenetic regulation of chromatin is crucial for the response to autophagy. Intriguingly, glucose starvation-induced PHF20-MLL3/4 complex can work in the distal regions and activate autophagy genes through enhancer activation. Histone H3K36me2 in enhancer regions is recognized by PHF20 through the Tudor 1 and 2 domains and this recognition is required for the activation of the transcription of autophagy genes, leading to the continued autophagic flux. Given that PHF20 plays an important role in stress-induced autophagy, connections between H3K36me2-enriched regions and enhancer activation by PHF20 reveal a new way in which cells cope with various harmful conditions.

As neither PHF20 protein level nor H3K36me2 level is increased by glucose starvation, we speculate that certain signal-induced post-translational modifications of PHF20 may contribute to the increased recruitment of PHF20 to H3K36me2-enriched chromatin regions during starvation-induced autophagy. Another possibility is that certain transcription factors and coregulators function to facilitate the enhanced binding of PHF20 to H3K36me2-enriched target sites. Since deletion of the Tudor domain of PHF20 led to the failure of PHF20 recruitment to the H3K36me2-enriched region, certain post-translational modifications of PHF20 may occur on the Tudor domain or nearby regions to make it effective for accommodating H3K36me2 binding. Moreover, we found that PHF20 Tudor domain also showed comparable binding to H4K20me2 and H3K27me2 from *in vitro* peptide binding array. In this study, we only focused on H3K36me2 to further studies, although it is possible that H4K20me2 or H3K27me2 might have functions to induce the binding of PHF20 to the target sites.

SET1 family methyltransferases including the MLL family proteins should be associated with WRAD components—which comprise WDR5, RbBP5, Ash2L and DPY-30—for their complete activation (74,75). WRAD induces the allosteric activation of methyltransferases or recruits methyltransferases to the appropriate target sites (76–79). Since the MLL complex is responsible for all three types of H3K4 methylations, each subtype of MLL complex possesses distinct enzymatic activity toward its substrate; MLL1/2 is a major methyltransferase for H3K4me3 on promoters (80,81), while MLL3/4 is responsible for the accumulation of H3K4me1 on active enhancers (82–84). Therefore, the genomic site where each subtype of the MLL complex is recruited under specific conditions should be tightly regulated. Our finding regarding the recruitment of WDR5 and RbBP5 by PHF20 to the target enhancer site suggests that PHF20 plays an important role in inducing H3K4 methylation via the MLL complex. Especially, our immunoprecipitation data shows that PHF20 has a binding preference to MLL3/4 complex compared to MLL1/2 complex (Figure 6B). Therefore, our data suggest that PHF20 with H3K36me2 binding activity might contribute to the regulation of the subtype-specific target decision between the MLL complexes, depending on the upstream signals.

The epigenetic and transcriptional control of autophagy is mainly triggered by upstream signaling cascades, and then regulated by epigenetic enzymes in the nucleus. Hi-

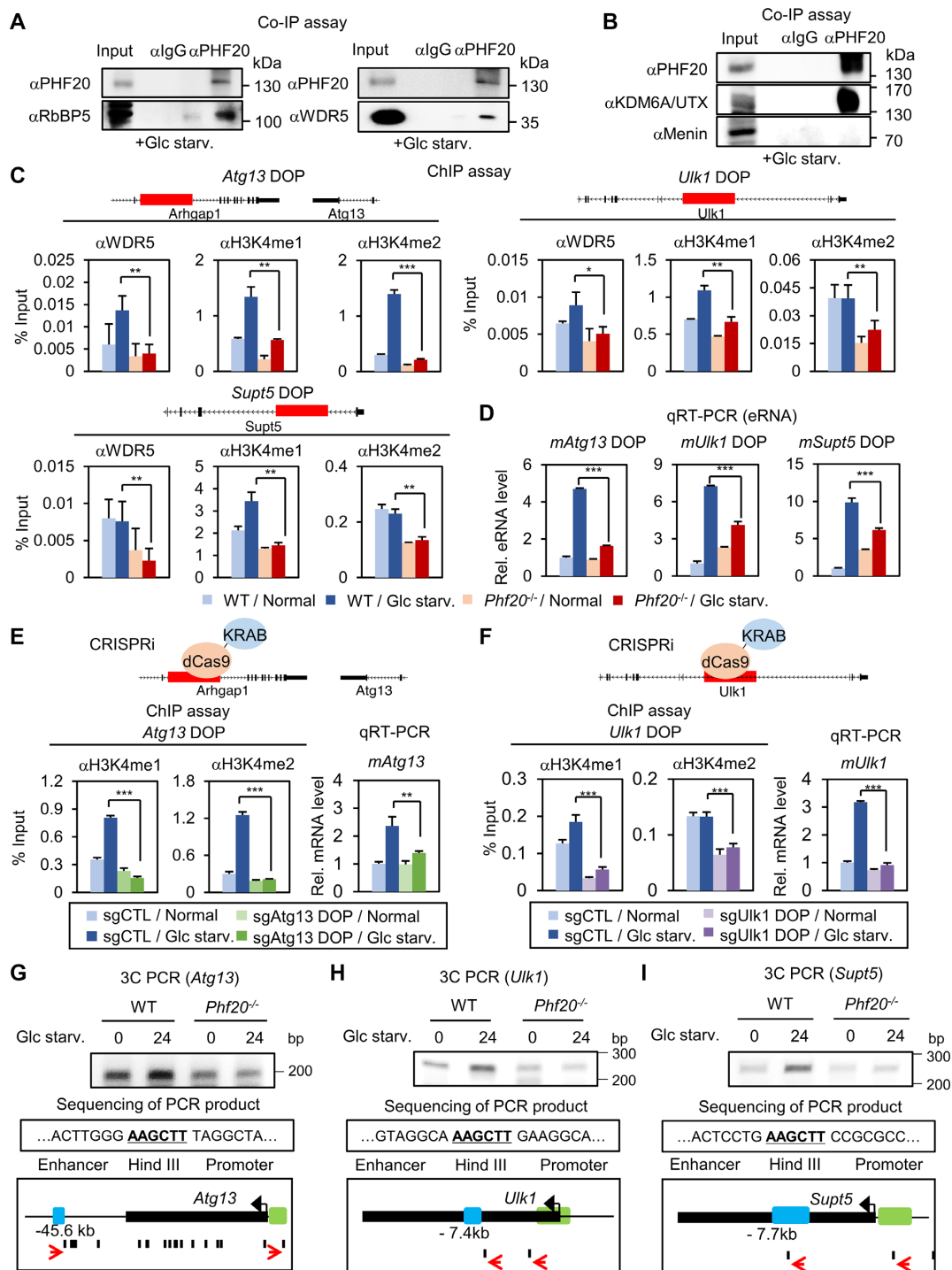


**Figure 6.** PHF20 activates enhancers by recruiting MLL3/4 complex. (A and B) Co-immunoprecipitation assay of endogenous PHF20 with WRAD components including WDR5 and RbBP5 (A) or MLL subtype specific components exemplified by Menin (MLL1/2 complex-specific) and KDM6A/UTX (MLL3/4 complex-specific) (B) under glucose starvation. (C) Chromatin immunoprecipitation (ChIP) assay was detected by individual qRT-PCR with primers for *Atg13*, *Ulk1* and *Supt5* DOP regions. Bars, mean  $\pm$  SEM; \*\*\*  $P < 0.001$ , \*\*  $P < 0.01$ . Statistical analysis using two-tailed t-test. (D) qRT-PCR for expression of enhancer RNA (eRNA) on *Atg13*, *Ulk1* and *Supt5* DOP regions. Bars, mean  $\pm$  SEM; \*\*\*  $P < 0.001$ . Statistical analysis using two-tailed t-test. (E) qRT-PCR for ChIP assay with histone H3K4me1 and H3K4me2 antibodies on *Atg13* DOP region (left panel) and qRT-PCR of *Atg13* mRNA (right panel). sg*Atg13* cell line was generated by CRISPRi system with sgRNA targeting *Atg13* DOP region. Bars, mean  $\pm$  SEM; \*\*\*  $P < 0.001$ , \*\*  $P < 0.01$ . Statistical analysis using two-tailed t-test. (F) qRT-PCR analysis after ChIP assay with H3K4me1 and H3K4me2 antibodies on *Ulk1* DOP region (left panel) and qRT-PCR of *Ulk1* mRNA (right panel). sg*Ulk1* cell line was generated by CRISPRi system with sgRNA targeting *Ulk1* DOP region. Bars, mean  $\pm$  SEM; \*\*\*  $P < 0.001$ . Statistical analysis using two-tailed t-test. (G-I) Chromosome conformation capture (3C) assay on promoter-enhancer region of PHF20 target genes including *Atg13* (G), *Ulk1* (H) and *Supt5* (I). PCR products were detected by DNA gel electrophoresis. DNA sequencing results were indicated (middle box). The models describe promoters (green blocks) with possible enhancer elements (blue blocks). Black lines represent HindIII restriction sites. Red arrows represent the site and the direction of primers used in PCR (bottom box).

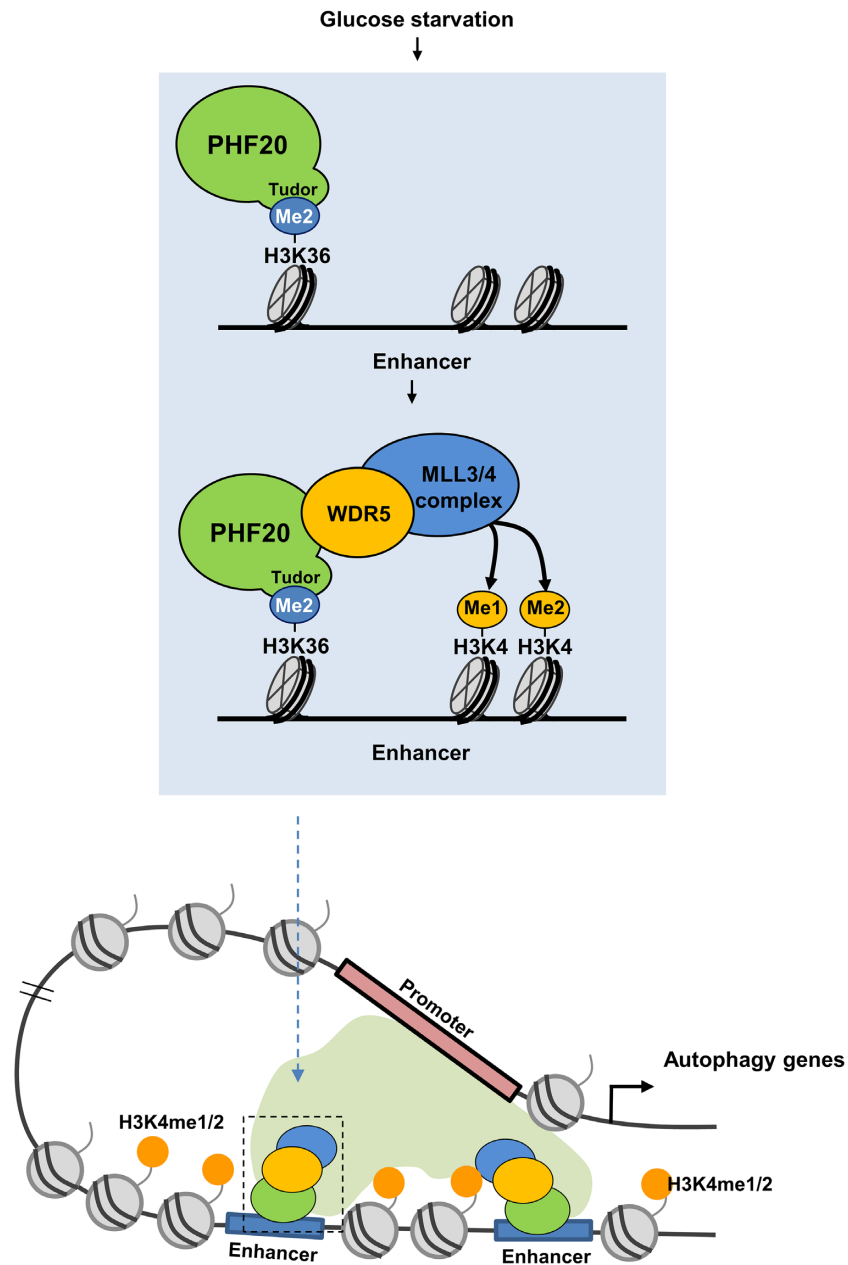


**Figure 7.** PHF20 is crucial for epigenetic regulation of autophagy via H3K36me2-dependent enhancer activation. Model of working mechanism of PHF20 in autophagy gene regulation via activation of enhancers that are co-occupied by H3K36me2.

stone modifications and epigenetic enzymes are linked to the transcriptional regulation of autophagy depending upstream signals. We have previously identified CARM1 arginine methyltransferase as an essential regulator of both TFEB and FOXO transcription factors. CARM1 directly functions as a coactivator for TFEB with increased H3R17 methylation. CARM1 also has a nonhistone substrate, Pontin, as well as a histone substrate, H3R17me2; methylated Pontin functions as a coactivator of FOXO, with increased H4 acetylation by the Tip60 coactivator (85). Compared to the specific PHF20 binding to an enhancer region, methylated Pontin can bind both the distal DNA region and the promoter region via FOXO3a binding. Although further studies are needed to understand how PHF20-dependent

enhancers and methylated Pontin-FOXO3a-dependent enhancers are orchestrated to work with promoters to regulate autophagy genes upon glucose starvation, our study suggests the possibility that there exist various ways of enhancer activation via a distinct signaling axis. We speculate that pharmacological manipulation would be helpful in controlling autophagy as well as autophagy-related diseases by selectively blocking transcription factors, coregulators and various signaling axes.

Various histone marks with their corresponding epigenetic writers, such as H3R17me2 and CARM1, H4K16ac and hMOF, H3K9me2 and G9a, and H3K27me3 and EZH2, which are involved in the epigenetic regulation of autophagy have been reported. Given that PHF20 is an epi-

genetic reader without possessing enzymatic activity, our studies extend the nuclear events of autophagy to highlight the role of epigenetic readers in recruiting epigenetic writers/erasers together to the target sites. Therefore, identification of autophagy-specific epigenetic writers/erasers and the corresponding epigenetic readers can both provide a basis for understanding the transcriptional outcome eliciting the autophagic process and be applicable to the development of therapeutic approaches for the dysregulated autophagic processes which lead to human diseases.

Our findings provide a novel insight into the function of PHF20 in regulating the expression of autophagy genes via the recognition of H3K36me2 and highlight the importance of enhancers in the regulation of autophagy genes. Furthermore, our findings will have application in future drug development research, such as in determining the therapeutic targets for autophagy-related diseases.

## DATA AVAILABILITY

RNA-seq, ChIP-seq, and ATAC-seq data have been deposited with the Gene Expression Omnibus (GEO) under accession number GSE193393. To characterize chromatin states of MEFs, chromHMM was performed with 12 previously published ChIP-seq data sets (CTCF: GSE36027, H3K27ac: GSE31039, GSE113429, H3K27me3: GSE26099, GSE26657, H3K36me2: GSE160266, H3K36me3: GSE26099, H3K4me1: GSE31039, H3K4me2: GSE90893, H3K4me3: GSE31039, GSE26657, H3K9ac: GSM2417089, H3K9me3: GSE26657, H4K16ac: GSE97459, PolIII: GSE36027).

## SUPPLEMENTARY DATA

Supplementary Data are available at NAR Online.

## ACKNOWLEDGEMENTS

*Phf20*<sup>-/-</sup> primary MEFs were kindly provided by Mark T. Bedford from MD Anderson Cancer Center.

*Author contributions:* S.W.P., J.K., S.O., J.L., J.C., H.S.L., K.I.K., D.P. and S.H.B. conceived and designed the research. S.W.P., S.O., J.L., J.C. and H.S.L. performed the experiments and J.K. and D.P. analyzed the bioinformatics data. S.W.P., J.K., S.O., D.P. and S.H.B. wrote the paper.

## FUNDING

Creative Research Initiatives Program (Research Center for Epigenetic Code and Diseases) [2017R1A3B1023387]; Science Research Center program [NRF-2016R1A5A1010764 to S.H.B.]; Basic Science Research Program [NRF-2019R1C1C1008181]; the Bio & Medical Technology Development Program [2022M3A9B6082670]; Ministry of Education [2021R1A6A1A10044950 to D.P.]; Science Research Center Program (Cellular Heterogeneity Research Center) [NRF-2016 R1A5A1011974 to K.I.K.] from the National Research Foundation (NRF) grant funded by the Korea government. Funding for open access charge: Creative Research Initiatives Program from NRF [2017R1A3B1023387].

*Conflict of interest statement.* None declared.

## REFERENCES

- Mizushima, N., Levine, B., Cuervo, A.M. and Klionsky, D.J. (2008) Autophagy fights disease through cellular self-digestion. *Nature*, **451**, 1069–1075.
- Klionsky, D.J. and Emr, S.D. (2000) Autophagy as a regulated pathway of cellular degradation. *Science*, **290**, 1717–1721.
- Yang, Z. and Klionsky, D.J. (2010) Eaten alive: a history of macroautophagy. *Nat. Cell Biol.*, **12**, 814–822.
- Lum, J.J., DeBerardinis, R.J. and Thompson, C.B. (2005) Autophagy in metazoans: cell survival in the land of plenty. *Nat. Rev. Mol. Cell Biol.*, **6**, 439–448.
- Levine, B. and Kroemer, G. (2008) Autophagy in the pathogenesis of disease. *Cell*, **132**, 27–42.
- Choi, A.M., Ryter, S.W. and Levine, B. (2013) Autophagy in human health and disease. *N. Engl. J. Med.*, **368**, 651–662.
- Glick, D., Barth, S. and Macleod, K.F. (2010) Autophagy: cellular and molecular mechanisms. *J. Pathol.*, **221**, 3–12.
- Mizushima, N. (2007) Autophagy: process and function. *Genes. Dev.*, **21**, 2861–2873.
- Baek, S.H. and Kim, K.I. (2017) Epigenetic control of autophagy: nuclear events gain more attention. *Mol. Cell*, **65**, 781–785.
- Fullgrave, J., Klionsky, D.J. and Joseph, B. (2014) The return of the nucleus: transcriptional and epigenetic control of autophagy. *Nat. Rev. Mol. Cell Biol.*, **15**, 65–74.
- Mammucari, C., Milan, G., Romanello, V., Masiero, E., Rudolf, R., Del Piccolo, P., Burden, S.J., Di Lisi, R., Sandri, C., Zhao, J. *et al.* (2007) FoxO3 controls autophagy in skeletal muscle in vivo. *Cell Metab.*, **6**, 458–471.
- Settembre, C., Di Malta, C., Polito, V.A., Garcia Arencibia, M., Vetrini, F., Erdin, S., Erdin, S.U., Huynh, T., Medina, D., Colella, P. *et al.* (2011) TFEB links autophagy to lysosomal biogenesis. *Science*, **332**, 1429–1433.
- Zhou, J., Liao, W., Yang, J., Ma, K., Li, X., Wang, Y., Wang, D., Wang, L., Zhang, Y., Yin, Y. *et al.* (2012) FOXO3 induces FOXO1-dependent autophagy by activating the AKT1 signaling pathway. *Autophagy*, **8**, 1712–1723.
- Heintzman, N.D., Stuart, R.K., Hon, G., Fu, Y., Ching, C.W., Hawkins, R.D., Barrera, L.O., Van Calcar, S., Qu, C., Ching, K.A. *et al.* (2007) Distinct and predictive chromatin signatures of transcriptional promoters and enhancers in the human genome. *Nat. Genet.*, **39**, 311–318.
- Greer, E.L. and Shi, Y. (2012) Histone methylation: a dynamic mark in health, disease and inheritance. *Nat. Rev. Genet.*, **13**, 343–357.
- Creyghton, M.P., Cheng, A.W., Welstead, G.G., Kooistra, T., Carey, B.W., Steine, E.J., Hanna, J., Lodato, M.A., Frampton, G.M., Sharp, P.A. *et al.* (2010) Histone H3K27ac separates active from poised enhancers and predicts developmental state. *Proc. Natl. Acad. Sci. U.S.A.*, **107**, 21931–21936.
- Alam, H., Gu, B. and Lee, M.G. (2015) Histone methylation modifiers in cellular signaling pathways. *Cell Mol. Life Sci.*, **72**, 4577–4592.
- Jeong, K.W., Kim, K., Situ, A.J., Ulmer, T.S., An, W. and Stallcup, M.R. (2011) Recognition of enhancer element-specific histone methylation by TIP60 in transcriptional activation. *Nat. Struct. Mol. Biol.*, **18**, 1358–1365.
- Purcell, D.J., Jeong, K.W., Bittencourt, D., Gerke, D.S. and Stallcup, M.R. (2011) A distinct mechanism for coactivator versus corepressor function by histone methyltransferase G9a in transcriptional regulation. *J. Biol. Chem.*, **286**, 41963–41971.
- Heinz, S., Romanoski, C.E., Benner, C. and Glass, C.K. (2015) The selection and function of cell type-specific enhancers. *Nat. Rev. Mol. Cell Biol.*, **16**, 144–154.
- Workman, J.L. and Abmayr, S.M. (2004) Histone H3 variants and modifications on transcribed genes. *Proc. Natl. Acad. Sci. U.S.A.*, **101**, 1429–1430.
- Biswas, S. and Rao, C.M. (2018) Epigenetic tools (The writers, the readers and the erasers) and their implications in cancer therapy. *Eur. J. Pharmacol.*, **837**, 8–24.
- Hyun, K., Jeon, J., Park, K. and Kim, J. (2017) Writing, erasing and reading histone lysine methylations. *Exp. Mol. Med.*, **49**, e324.
- Suganuma, T. and Workman, J.L. (2008) Crosstalk among histone modifications. *Cell*, **135**, 604–607.

25. Artal-Martinez de Narvajias, A., Gomez, T.S., Zhang, J.S., Mann, A.O., Taoda, Y., Gorman, J.A., Herreros-Villanueva, M., Gress, T.M., Ellenrieder, V., Bujanda, L. *et al.* (2013) Epigenetic regulation of autophagy by the methyltransferase G9a. *Mol. Cell Biol.*, **33**, 3983–3993.
26. Fullgrabe, J., Lynch-Day, M.A., Heldring, N., Li, W., Struijk, R.B., Ma, Q., Hermanson, O., Rosenfeld, M.G., Klionsky, D.J. and Joseph, B. (2013) The histone H4 lysine 16 acetyltransferase hMOF regulates the outcome of autophagy. *Nature*, **500**, 468–471.
27. Wei, F.Z., Cao, Z., Wang, X., Wang, H., Cai, M.Y., Li, T., Hattori, N., Wang, D., Du, Y., Song, B. *et al.* (2015) Epigenetic regulation of autophagy by the methyltransferase EZH2 through an mTOR-dependent pathway. *Autophagy*, **11**, 2309–2322.
28. Yi, C., Ma, M., Ran, L., Zheng, J., Tong, J., Zhu, J., Ma, C., Sun, Y., Zhang, S., Feng, W. *et al.* (2012) Function and molecular mechanism of acetylation in autophagy regulation. *Science*, **336**, 474–477.
29. Shin, H.J., Kim, H., Oh, S., Lee, J.G., Kee, M., Ko, H.J., Kweon, M.N., Won, K.J. and Baik, S.H. (2016) AMPK-SKP2-CARM1 signalling cascade in transcriptional regulation of autophagy. *Nature*, **534**, 553–557.
30. Lan, F., Collins, R.E., De Cegli, R., Alpatov, R., Horton, J.R., Shi, X., Gozani, O., Cheng, X. and Shi, Y. (2007) Recognition of unmethylated histone H3 lysine 4 links BHC80 to LSD1-mediated gene repression. *Nature*, **448**, 718–722.
31. Pena, P.V., Davrazou, F., Shi, X., Walter, K.L., Verkhusha, V.V., Gozani, O., Zhao, R. and Kutateladze, T.G. (2006) Molecular mechanism of histone H3K4me3 recognition by plant homeodomain of ING2. *Nature*, **442**, 100–103.
32. Hung, T., Binda, O., Champagne, K.S., Kuo, A.J., Johnson, K., Chang, H.Y., Simon, M.D., Kutateladze, T.G. and Gozani, O. (2009) ING4 mediates crosstalk between histone H3 K4 trimethylation and H3 acetylation to attenuate cellular transformation. *Mol. Cell*, **33**, 248–256.
33. Shi, X., Hong, T., Walter, K.L., Ewalt, M., Michishita, E., Hung, T., Carney, D., Pena, P., Lan, F., Kaadige, M.R. *et al.* (2006) ING2 PHD domain links histone H3 lysine 4 methylation to active gene repression. *Nature*, **442**, 96–99.
34. Nourani, A., Howe, L., Pray-Grant, M.G., Workman, J.L., Grant, P.A. and Cote, J. (2003) Opposite role of yeast ING family members in p53-dependent transcriptional activation. *J. Biol. Chem.*, **278**, 19171–19175.
35. Yun, M., Wu, J., Workman, J.L. and Li, B. (2011) Readers of histone modifications. *Cell Res.*, **21**, 564–578.
36. Cui, G., Park, S., Badeaux, A.I., Kim, D., Lee, J., Thompson, J.R., Yan, F., Kaneko, S., Yuan, Z., Botuyan, M.V. *et al.* (2012) PHF20 is an effector protein of p53 double lysine methylation that stabilizes and activates p53. *Nat. Struct. Mol. Biol.*, **19**, 916–924.
37. Cai, Y., Jin, J., Swanson, S.K., Cole, M.D., Choi, S.H., Florens, L., Washburn, M.P., Conaway, J.W. and Conaway, R.C. (2010) Subunit composition and substrate specificity of a MOF-containing histone acetyltransferase distinct from the male-specific lethal (MSL) complex. *J. Biol. Chem.*, **285**, 4268–4272.
38. Li, X., Wu, L., Corsa, C.A., Kunkel, S. and Dou, Y. (2009) Two mammalian MOF complexes regulate transcription activation by distinct mechanisms. *Mol. Cell*, **36**, 290–301.
39. Taipale, M., Rea, S., Richter, K., Vilar, A., Lichter, P., Imhof, A. and Akhtar, A. (2005) hMOF histone acetyltransferase is required for histone H4 lysine 16 acetylation in mammalian cells. *Mol. Cell Biol.*, **25**, 6798–6810.
40. Shia, W.J., Pattenden, S.G. and Workman, J.L. (2006) Histone H4 lysine 16 acetylation breaks the genome's silence. *Genome Biol.*, **7**, 217.
41. Klein, B.J., Wang, X., Cui, G., Yuan, C., Botuyan, Maria V., Lin, K., Lu, Y., Wang, X., Zhao, Y., Bruns, C.J. *et al.* (2016) PHF20 readers link methylation of histone H3K4 and p53 with H4K16 acetylation. *Cell Rep.*, **17**, 1158–1170.
42. Zhang, X., Peng, D., Xi, Y., Yuan, C., Sagum, C.A., Klein, B.J., Tanaka, K., Wen, H., Kutateladze, T.G., Li, W. *et al.* (2016) G9a-mediated methylation of ER $\alpha$  links the PHF20/MOF histone acetyltransferase complex to hormonal gene expression. *Nat. Commun.*, **7**, 10810.
43. Zhang, T., Ah Park, K., Li, Y., Sun Byun, H., Jeon, J., Lee, Y., Hee Hong, J., Man Kim, J., Huang, S.-M., Choi, S.-W. *et al.* (2013) PHF20 regulates NF- $\kappa$ B signalling by disrupting recruitment of PP2A to p65. *Nat. Commun.*, **4**, 2062.
44. Badeaux, A.I., Yang, Y., Cardenas, K., Vemulapalli, V., Chen, K., Kusewitt, D., Richie, E., Li, W. and Bedford, M.T. (2012) Loss of the methyl lysine effector protein PHF20 impacts the expression of genes regulated by the lysine acetyltransferase MOF. *J. Biol. Chem.*, **287**, 429–437.
45. Bolger, A.M., Lohse, M. and Usadel, B. (2014) Trimmomatic: a flexible trimmer for illumina sequence data. *Bioinformatics*, **30**, 2114–2120.
46. Dobin, A., Davis, C.A., Schlesinger, F., Drenkow, J., Zaleski, C., Jha, S., Batut, P., Chaisson, M. and Gingeras, T.R. (2013) STAR: ultrafast universal RNA-seq aligner. *Bioinformatics*, **29**, 15–21.
47. Li, B. and Dewey, C.N. (2011) RSEM: accurate transcript quantification from RNA-Seq data with or without a reference genome. *BMC Bioinformatics*, **12**, 323.
48. Huang da, W., Sherman, B.T. and Lempicki, R.A. (2009) Bioinformatics enrichment tools: paths toward the comprehensive functional analysis of large gene lists. *Nucleic Acids Res.*, **37**, 1–13.
49. Subramanian, A., Tamayo, P., Mootha, V.K., Mukherjee, S., Ebert, B.L., Gillette, M.A., Paulovich, A., Pomeroy, S.L., Golub, T.R., Lander, E.S. *et al.* (2005) Gene set enrichment analysis: a knowledge-based approach for interpreting genome-wide expression profiles. *Proc. Natl. Acad. Sci. U.S.A.*, **102**, 15545–15550.
50. Smedley, D., Haider, S., Ballester, B., Holland, R., London, D., Thorisson, G. and Kasprzyk, A. (2009) BioMart—biological queries made easy. *BMC Genomics*, **10**, 22.
51. Liberzon, A., Subramanian, A., Pinchback, R., Thorvaldsdottir, H., Tamayo, P. and Mesirov, J.P. (2011) Molecular signatures database (MSigDB) 3.0. *Bioinformatics*, **27**, 1739–1740.
52. Liberzon, A., Birger, C., Thorvaldsdottir, H., Ghandi, M., Mesirov, J.P. and Tamayo, P. (2015) The molecular signatures database (MSigDB) hallmark gene set collection. *Cell Syst.*, **1**, 417–425.
53. Li, H. and Durbin, R. (2009) Fast and accurate short read alignment with burrows-wheeler transform. *Bioinformatics*, **25**, 1754–1760.
54. Zhang, Y., Liu, T., Meyer, C.A., Eeckhoutte, J., Johnson, D.S., Bernstein, B.E., Nusbaum, C., Myers, R.M., Brown, M., Li, W. *et al.* (2008) Model-based analysis of chip-Seq (MACS). *Genome Biol.*, **9**, R137.
55. Quinlan, A.R. and Hall, I.M. (2010) BEDTools: a flexible suite of utilities for comparing genomic features. *Bioinformatics*, **26**, 841–842.
56. Love, M.I., Huber, W. and Anders, S. (2014) Moderated estimation of fold change and dispersion for RNA-seq data with DESeq2. *Genome Biol.*, **15**, 550.
57. Ramirez, F., Ryan, D.P., Gruning, B., Bhardwaj, V., Kilpert, F., Richter, A.S., Heyne, S., Dundar, F. and Manke, T. (2016) deepTools2: a next generation web server for deep-sequencing data analysis. *Nucleic Acids Res.*, **44**, W160–W165.
58. Hagege, H., Klous, P., Braem, C., Splinter, E., Dekker, J., Cathala, G., de Laat, W. and Forne, T. (2007) Quantitative analysis of chromosome conformation capture assays (3C-qPCR). *Nat. Protoc.*, **2**, 1722–1733.
59. Naumova, N., Smith, E.M., Zhan, Y. and Dekker, J. (2012) Analysis of long-range chromatin interactions using chromosome conformation capture. *Methods*, **58**, 192–203.
60. Ernst, J. and Kellis, M. (2012) ChromHMM: automating chromatin-state discovery and characterization. *Nat Methods*, **9**, 215–216.
61. Ernst, J. and Kellis, M. (2017) Chromatin-state discovery and genome annotation with ChromHMM. *Nat. Protoc.*, **12**, 2478–2492.
62. Adams-Cioaba, M.A., Li, Z., Tempel, W., Guo, Y., Bian, C., Li, Y., Lam, R. and Min, J. (2012) Crystal structures of the tudor domains of human PHF20 reveal novel structural variations on the royal family of proteins. *FEBS Lett.*, **586**, 859–865.
63. Cai, L., Rothbart, S.B., Lu, R., Xu, B., Chen, W.Y., Tripathy, A., Rockowitz, S., Zheng, D., Patel, D.J., Allis, C.D. *et al.* (2013) An H3K36 methylation-engaging tudor motif of polycomb-like proteins mediates PRC2 complex targeting. *Mol. Cell*, **49**, 571–582.
64. Meers, M.P., Bryson, T.D., Henikoff, J.G. and Henikoff, S. (2019) Improved CUT&RUN chromatin profiling tools. *Elife*, **8**, e46314.
65. Hainer, S.J. and Fazzio, T.G. (2019) High-Resolution chromatin profiling using CUT&RUN. *Curr. Protoc. Mol. Biol.*, **126**, e85.
66. Smith, E., Lin, C. and Shilatifard, A. (2011) The super elongation complex (SEC) and MLL in development and disease. *Genes Dev.*, **25**, 661–672.
67. Dou, Y., Milne, T.A., Tackett, A.J., Smith, E.R., Fukuda, A., Wysocka, J., Allis, C.D., Chait, B.T., Hess, J.L. and Roeder, R.G. (2005) Physical association and coordinate function of the H3 K4

- methyltransferase MLL1 and the H4 K16 acetyltransferase MOF. *Cell*, **121**, 873–885.
68. Milne, T.A., Briggs, S.D., Brock, H.W., Martin, M.E., Gibbs, D., Allis, C.D. and Hess, J.L. (2002) MLL targets SET domain methyltransferase activity to hox gene promoters. *Mol. Cell*, **10**, 1107–1117.
69. Jeong, K.W., Andreu-Vieyra, C., You, J.S., Jones, P.A. and Stallcup, M.R. (2014) Establishment of active chromatin structure at enhancer elements by mixed-lineage leukemia 1 to initiate estrogen-dependent gene expression. *Nucleic Acids Res.*, **42**, 2245–2256.
70. Shilatifard, A. (2012) The COMPASS family of histone H3K4 methylases: mechanisms of regulation in development and disease pathogenesis. *Annu. Rev. Biochem.*, **81**, 65–95.
71. Wang, D., Garcia-Bassets, I., Benner, C., Li, W., Su, X., Zhou, Y., Qiu, J., Liu, W., Kaikkonen, M.U., Ohgi, K.A. *et al.* (2011) Reprogramming transcription by distinct classes of enhancers functionally defined by eRNA. *Nature*, **474**, 390–394.
72. Li, W., Notani, D., Ma, Q., Tanasa, B., Nunez, E., Chen, A.Y., Merkurjev, D., Zhang, J., Ohgi, K., Song, X. *et al.* (2013) Functional roles of enhancer RNAs for oestrogen-dependent transcriptional activation. *Nature*, **498**, 516–520.
73. Thakore, P.I., D'Ippolito, A.M., Song, L., Safi, A., Shivakumar, N.K., Kabadi, A.M., Reddy, T.E., Crawford, G.E. and Gersbach, C.A. (2015) Highly specific epigenome editing by CRISPR-Cas9 repressors for silencing of distal regulatory elements. *Nat. Methods*, **12**, 1143–1149.
74. Miller, T., Krogan, N.J., Dover, J., Erdjument-Bromage, H., Tempst, P., Johnston, M., Greenblatt, J.F. and Shilatifard, A. (2001) COMPASS: a complex of proteins associated with a trithorax-related SET domain protein. *Proc. Natl. Acad. Sci. U.S.A.*, **98**, 12902–12907.
75. Ernst, P. and Vakoc, C.R. (2012) WRAD: enabler of the SET1-family of H3K4 methyltransferases. *Brief. Funct. Genomics*, **11**, 217–226.
76. Patel, A., Dharmarajan, V., Vought, V.E. and Cosgrove, M.S. (2009) On the mechanism of multiple lysine methylation by the human mixed lineage leukemia protein-1 (MLL1) core complex. *J. Biol. Chem.*, **284**, 24242–24256.
77. Patel, A., Vought, V.E., Dharmarajan, V. and Cosgrove, M.S. (2011) A novel non-SET domain multi-subunit methyltransferase required for sequential nucleosomal histone H3 methylation by the mixed lineage leukemia protein-1 (MLL1) core complex. *J. Biol. Chem.*, **286**, 3359–3369.
78. Steward, M.M., Lee, J.S., O'Donovan, A., Wyatt, M., Bernstein, B.E. and Shilatifard, A. (2006) Molecular regulation of H3K4 trimethylation by ASH2L, a shared subunit of MLL complexes. *Nat. Struct. Mol. Biol.*, **13**, 852–854.
79. Bryk, M., Cao, F., Chen, Y., Cierpicki, T., Liu, Y., Basrur, V., Lei, M. and Dou, Y. (2010) An Ash2L/rbbp5 heterodimer stimulates the MLL1 methyltransferase activity through coordinated substrate interactions with the MLL1 SET domain. *PLoS ONE*, **5**, e14102.
80. Hu, D., Garruss, A.S., Gao, X., Morgan, M.A., Cook, M., Smith, E.R. and Shilatifard, A. (2013) The mll2 branch of the COMPASS family regulates bivalent promoters in mouse embryonic stem cells. *Nat. Struct. Mol. Biol.*, **20**, 1093–1097.
81. Wang, P., Lin, C., Smith, E.R., Guo, H., Sanderson, B.W., Wu, M., Gogol, M., Alexander, T., Seidel, C., Wiedemann, L.M. *et al.* (2009) Global analysis of H3K4 methylation defines MLL family member targets and points to a role for MLL1-mediated H3K4 methylation in the regulation of transcriptional initiation by RNA polymerase II. *Mol. Cell Biol.*, **29**, 6074–6085.
82. Lee, J.E., Wang, C., Xu, S., Cho, Y.W., Wang, L., Feng, X., Baldrige, A., Sartorelli, V., Zhuang, L., Peng, W. *et al.* (2013) H3K4 mono- and di-methyltransferase MLL4 is required for enhancer activation during cell differentiation. *Elife*, **2**, e01503.
83. Herz, H.M., Mohan, M., Garruss, A.S., Liang, K., Takahashi, Y.H., Mickey, K., Voets, O., Verrijzer, C.P. and Shilatifard, A. (2012) Enhancer-associated H3K4 monomethylation by Trithorax-related, the drosophila homolog of mammalian mll3/mll4. *Genes Dev.*, **26**, 2604–2620.
84. Liu, Y., Qin, S., Chen, T.Y., Lei, M., Dhar, S.S., Ho, J.C., Dong, A., Loppnau, P., Li, Y., Lee, M.G. *et al.* (2019) Structural insights into trans-histone regulation of H3K4 methylation by unique histone H4 binding of MLL3/4. *Nat. Commun.*, **10**, 36.
85. Yu, Y.S., Shin, H.R., Kim, D., Baek, S.A., Choi, S.A., Ahn, H., Shamim, A., Kim, J., Kim, I.S., Kim, K.K. *et al.* (2020) Pontin arginine methylation by CARM1 is crucial for epigenetic regulation of autophagy. *Nat. Commun.*, **11**, 6297.